IL NUOVO CIMENTO Vol. 35 C, N. 6 Novembre-Dicembre 2012
DOI 10.1393/ncc/i2012-11380-8

Colloquia: LaThuile12

Precision measurement of the W boson mass at CDF

B. Jayatilaka on behalf of the CDF Collaboration
Duke University - Durham, NC, USA

ricevuto il 7 Settembre 2012

Summary. — A measurement of the mass of the W boson, M_W, is presented using $2.2\,\text{fb}^{-1}$ of the data from $p\bar{p}$ collisions at $\sqrt{s} = 1.96\,\text{TeV}$ collected with the CDF II detector at the Fermilab Tevatron. The mass is determined by fitting simulated signal and background distributions to 470126 W candidates decaying to $e\nu_e$ and 624708 decaying to $\mu\nu_\mu$. The result is $M_W = 80387 \pm 19\,\text{MeV}$ and is the most precise determination of the mass to date.

PACS 14.70.Fm – W bosons.
PACS 12.15.Ji – Applications of electroweak models to specific processes.
PACS 13.38.Be – Decays of W bosons.

1. – Introduction

The mass of the W boson (M_W) is an important parameter of the standard model (SM). Precise measurements of M_W and of the top quark mass (m_t) significantly constrain the mass of the, as yet, unobserved Higgs boson. Prior to the measurement presented here, the world average of $M_W = 80.399 \pm 0.023\,\text{GeV}$([1]) and $m_t = 173.2 \pm 0.9\,\text{GeV}$, yielded a limit on the SM Higgs boson mass of $M_H < 161\,\text{GeV}$ at 95% confidence level (CL).

The previous measurement of M_W by the CDF Collaboration was determined to be $M_W = 80.413 \pm 0.048\,\text{GeV}$ [1] from $200\,\text{pb}^{-1}$ of data while a recent measurement by the DØ Collaboration from $1\,\text{fb}^{-1}$ of data gave $M_W = 80.401 \pm 0.043\,\text{GeV}$ [2]. Presented here is the most recent measurement made by CDF, utilizing data corresponding to $2.2\,\text{fb}^{-1}$ of integrated luminosity.

2. – Analysis strategy

At the Tevatron, W bosons are primarily produced in $q\bar{q}$ annihilation, $q\bar{q} \to W + X$, where X can include QCD radiation that results in measurable hadronic recoil in events.

([1]) We use units where $c = 1$ throughout.

$W \to l\nu_l$ decays, where $l = e$ or μ, are selected with high purity by the CDF detector and used to measure M_W. As the longitudinal momentum of the neutrino is not measured, we use transverse([2]) components of charged lepton momentum (p_T^l), neutrino momentum (p_T^ν) and the transverse mass,

$$m_T = \sqrt{2p_T(l)p_T(\nu)[1 - \cos(\phi_l - \phi_\nu)]}, \tag{1}$$

which depend only on measurable quantities of the W decay, to measure M_W. A Monte Carlo simulation is used to predict the shape of these distributions as a function of M_W. A binned maximum-likelihood fit of these predictions to the data is used to determine the W boson mass.

These line-shape predictions depend on the kinematic distributions of the W decay products and detector effects, which are constrained from control samples and theoretical calculations. The kinematic distributions are determined by several effects including internal QED radiation, the intrinsic W boson transverse momentum, and the proton parton distribution functions (PDFs). Detector effects include external bremsstrahlung and ionisation energy loss in the detector material, tracker momentum scale, calorimeter energy scale, resolutions of the tracker and calorimeter, and the detector acceptance. A sophisticated, fast simulation has been developed that enables a study of these effects at a level below 1 part in 10^4.

3. – Event generation and simulation

W boson events are generated with the RESBOS Monte Carlo [3], which captures the relevant QCD physics and models the W p_T spectrum. QED processes, including final-state photon radiation, are simulated using PHOTOS [4], and are cross-checked against HORACE [5].

Non-perturbative physics, which are described by parameters that must be determined from experimental data, affect the shape of the W boson p_T. We determine these parameters from a fit to the dilepton spectra of $Z \to ee$ and $Z \to \mu\mu$ candidate events.

Parton distribution functions (PDFs) affect the W boson mass measurement through their effects on the kinematics of the decay charged lepton and because the measurement only uses charged leptons in a restricted rapidity range. The uncertainty arising from the PDFs is evaluated using the 68% CL MSTW2008 [6] error set. This is cross-checked by comparing the 90% CL CTEQ6.6 [7] error set with the 90% CL MSTW2008 error set.

The tracker and calorimeter response and the electron and muon acceptance are simulated using a parameterized fast detector simulation. Tracks in the CDF drift chamber associated with electrons and muons are simulated at the hit level. Electrons and muons are propagated along a helical trajectory from the production point, stepping through the layers of passive material, whose effects are simulated. The most relevant processes are ionisation energy loss for muons, bremsstrahlung ($e \to e\gamma$) for electrons, and conversion ($\gamma \to e^+e^-$) for photons. Multiple Coulomb scattering is simulated in order to incorporate its effect on track resolution.

([2]) CDF uses a cylindrical coordinate system with the z axis along the proton beam axis. Pseudorapidity is $\eta \equiv -\ln(\tan(\theta/2))$, where θ is the polar angle, and ϕ is the azimuthal angle relative to the proton beam direction, while $p_T = |p| \sin(\theta)$, $E_T = E \sin(\theta)$.

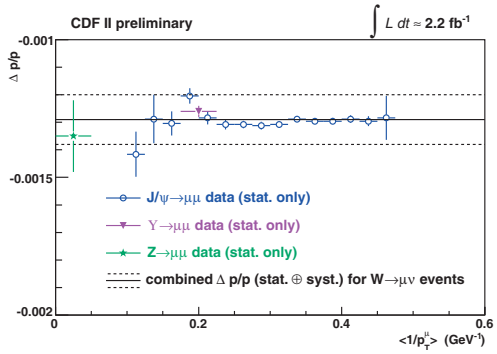

Fig. 1. – The fractional momentum correction for data as a function of the mean inverse momentum of muons from J/ψ, $\Upsilon(1S)$, and Z boson data.

The deposition of electromagnetic energy in the calorimeter for leptons and photons is simulated using parameterizations for the energy scale and resolution; energy loss in the solenoidal coil and due to longitudinal leakage; and non-linear response. The parameters for the scale and resolution, and the non-linearity, are fit from the data.

4. – Event selection

The event selection criteria for the W boson mass measurement are optimized to produce a sample with low background and which can be accurately modeled. W and Z boson candidates are selected by requiring the charged leptons have p_T greater than 30 GeV. Muon candidates are required to have hits in the muon detectors and electron candidates must have an E/p value of less than 1.6. Additionally two leptons of the same flavor and opposite charge as well as the mass of the dilepton system to be in the range $66 < m_{ll} < 116\,\text{GeV}$ are required for Z candidates. For W boson candidates, the recoil energy in the calorimeter is required to be less than 15 GeV, $\not\!\!E_T > 30\,\text{GeV}$ and $60 < m_T < 100\,\text{GeV}$. These selection criteria are applied to data collected between February 2002 and September 2007. The data correspond to an integrated luminosity of $2.2\,\text{fb}^{-1}$. The selection criteria yield 470126 $W \to e\nu$ candidates and 624708 $W \to \mu\nu$ candidates.

5. – Momentum scale calibration

The high-statistics $J/\psi \to \mu\mu$ and $\Upsilon(1S) \to \mu\mu$ quarkonia decays, along with the $Z \to \mu\mu$ sample, are used to set the momentum scale. The momentum scale is extracted from a binned maximum-likelihood fit of the data to simulated invariant-mass templates generated using the world average values.

The J/ψ sample has the advantage that its cross section is sufficiently large to enable a study of the momentum scale as a function of other variables. The $\Upsilon(1S)$ resonance has an invariant mass three times larger than the J/ψ, and supplies an intermediate reference point to study the momentum dependence of the momentum scale. The Υ hadrons also have the advantage that they are all produced promptly, allowing a study of the momentum scale using tracks that are beam-constrained in the same way as the tracks in the W and Z samples. The consistency of the momentum correction obtained

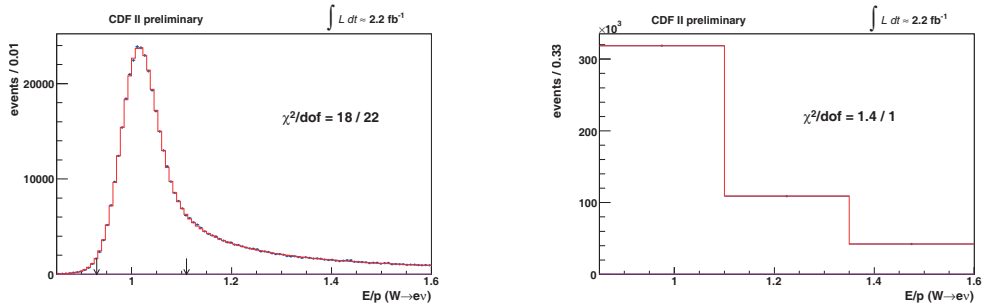

Fig. 2. – The E/p distribution of the $W \to e\nu$ data (points) used to determine the calorimeter energy scale (left) and to scale the radiative material in the simulation (right). The arrows indicate the fitting range used for the electron energy calibration.

from fits to J/ψ and Υ data can be seen in fig. 1. The combined momentum scale obtained from the J/ψ and Υ samples is applied to the W and Z samples.

The $Z \to \mu\mu$ mass fit is shown in fig. 3 (left), along with the statistical uncertainty and fit χ^2. A value of $m_Z = 91180 \pm 12_{\text{stat}} \pm 10_{\text{syst}}\,\text{MeV}$ is obtained, consistent with the world average value of $m_Z = 91188 \pm 2\,\text{MeV}$ [8]. The final momentum scale applied to the W boson data is obtained from combining the J/ψ, Υ, and Z measurements.

The tracking resolution is parameterized in the simulation by the tracking chamber hit resolution $\sigma_h = 150 \pm 3\,\mu\text{m}$ and the beamspot size $\sigma_b = 35 \pm 3\,\mu\text{m}$, which affects track resolution through the beam-constraint in the track fit. We fix σ_h with the non-beam-constrained $\Upsilon(1S)$ mass distribution and σ_b with the beam-constrained Z mass distribution.

6. – Energy scale calibration

The electron cluster is simulated by merging energies of the primary electron and proximate bremsstrahlung photons and conversion electrons. The distribution of electron and photon energy loss in the solenoid coil and leakage into the hadronic calorimeter are determined using GEANT.

The electromagnetic calorimeter energy scale is set using the peak of the E/p electron distribution from $W \to e\nu$ events (fig. 2, left) and $Z \to ee$ events. The electromagnetic calorimeter non-linearity is determined from E/p fits as a function of transverse energy from the $W \to e\nu$ and $Z \to ee$ samples. The tail of the E/p distribution is used to tune the absolute number of radiation lengths in the tracker material, as shown in fig. 2 (right).

The electromagnetic calorimeter resolution is parameterized as

$$\sigma_E/E = 12.6\%/\sqrt{E_T} \oplus \kappa, \tag{2}$$

where κ is the non-stochastic term in the resolution. Two κs are defined. The first, κ_e, defines the smearing of the primary high-E_T electron and is tuned from the peak region of the E/p distribution. The second, κ_γ, smears the energy contribution of each of the secondary electromagnetic particles: the bremsstrahlung photons and the conversion electrons. κ_γ is tuned on the width of the $Z \to ee$ distribution selected using high E/p ($E/p > 1.06$) electrons.

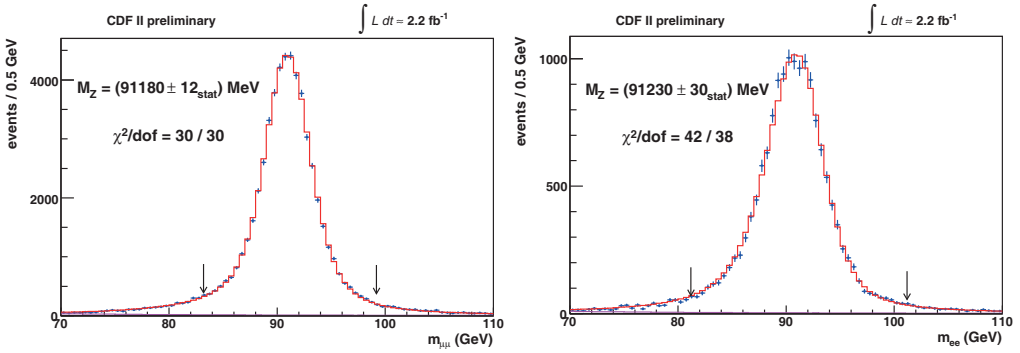

Fig. 3. – The maximum-likelihood fit to the $Z \to \mu\mu$ (left) and $Z \to ee$ (right) mass peaks, with the fitted mass values. The data (points) are shown along with the best-fit simulation template (histogram). The arrows indicate the fitting range.

The $Z \to ee$ mass is fitted to cross-check the energy scale and the non-linearity (fig. 3, right). A value of $m_Z = 91230 \pm 30_{\rm stat} \pm 14_{\rm syst}$ MeV is obtained, consistent with the world average. Thus, the measurements from E/p and the $Z \to ee$ mass are combined to obtain the final energy scale, applied to $W \to e\nu$ data.

7. – Recoil calibration

All particles recoiling against the W or Z boson are collectively referred to as the recoil. The recoil vector $\mathbf{u}$ is defined as the vector sum of transverse energy over all electromagnetic and hadronic calorimeter towers in the detector range $|\eta| < 2.4$. The calorimeter towers associated with the leptons are explicitly removed from the recoil calculation. A combination of minimum bias data and $Z \to ll$ data is used to model the behavior of the hadronic recoil, and $W \to l\nu$ data is used to cross-check the data corrections and the simulation.

The response of the calorimeter to the hadronic recoil is described by a response function, R, which scales the true recoil magnitude to simulate the measured magnitude.

The recoil resolution is assumed to have two components, which are summed vectorially: a "sampling" term representing the calorimeter "jet" resolution, and an underlying event component from the spectator and additional $p\bar{p}$ interactions.

$Z \to \mu\mu$ and $Z \to ee$ events are used to tune the recoil response and resolution parameters. The η axis is defined to be the geometric bisector of the two leptons and the ξ axis to be perpendicular to η. We project the vector p_T-balance onto the η and ξ axes and compare the data distribution to the simulation. Figure 4 shows the mean (left) and RMS (right) of the p_T-balancing in $Z \to ee$ events as a function of Z boson p_T.

8. – Backgrounds

Backgrounds passing the event selection cuts have different kinematic distributions from the W signal, and are therefore included in the template fits. The backgrounds to the $W \to \mu\nu$ and $W \to e\nu$ samples come from hadronic jet production, decays in flight, Z production, $W \to \tau\nu$ decays, and cosmic rays. The background rates and kinematics are determined using a combination of Monte-Carlo–based and data-based

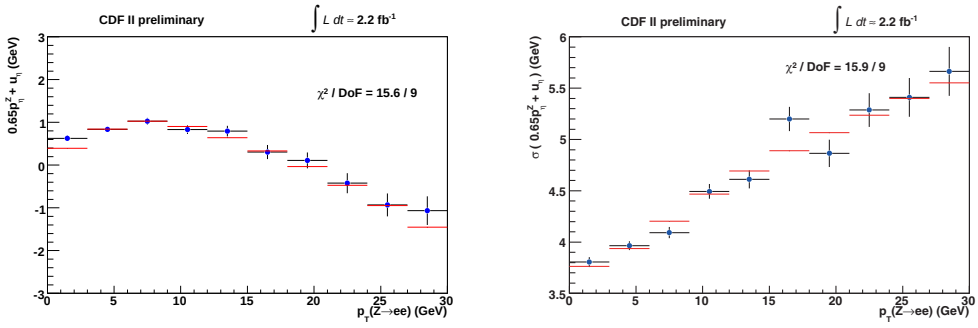

Fig. 4. – Mean value (left) and RMS (right) of the scaled p_T-balance projected onto the η axis as a function of $p_T(ll)$ for $Z \to ee$.

methods. Background fractions for the muon (electron) datasets are evaluated to be 7.35% (0.14%) from Z decays, 0.88% (0.93%) from $W \to \tau\nu$ decays, 0.04% (0.39%) from hadronic jets, 0.24% from DIF, and 0.02% from cosmic rays.

9. – Results and conclusions

The W boson mass is measured by performing a binned maximum-likelihood fit to the lepton p_T, neutrino p_T, and m_T distributions for each lepton channel. 1600 signal templates for M_W are generated between 80 GeV and 81 GeV and background templates are added with the shapes and normalisations described in sect. **8**. The final fit values were hidden during analysis by adding an unknown offset in the range $[-75{,}75]$ MeV. The results of the fits to the m_T (fig. 5), p_T^l, and p_T^ν kinematic distributions for both the electron and muon channels are summarized in table I.

Fits of simulated data to Monte Carlo templates have been performed to measure the statistical correlation between the fits to the m_T, p_T^l and p_T^ν distributions. The final results are combined, taking these correlations into account, using the BLUE [9] method.

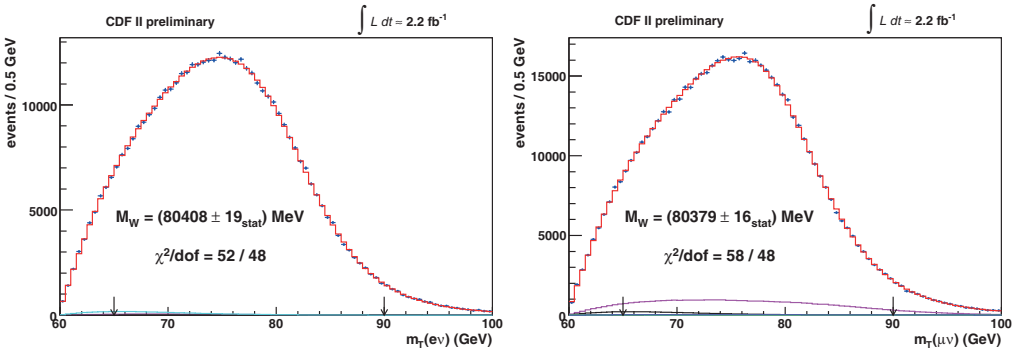

Fig. 5. – The W transverse mass fits for the electron (left) and muon (right) channels. The data (points) are shown along with the best-fit simulation template (red histogram). The background contributions to the template, including $Z \to ll$ (magenta histogram) and hadronic jets (cyan histogram), are overlaid. The arrows indicate the fitting range.

TABLE I. – *Fit results and uncertainties for M_W. The fit windows are* 65–90 GeV *for the m_T fit and* 32–48 GeV *for the p_T^ℓ and p_T^ν fits. The χ^2 of the fit is computed using the expected statistical errors on the data points.*

Distribution	W-boson mass (MeV)	χ^2/dof
$m_T(e,\nu)$	$80\,408 \pm 19_{\text{stat}} \pm 18_{\text{syst}}$	52/48
$p_T^\ell(e)$	$80\,393 \pm 21_{\text{stat}} \pm 19_{\text{syst}}$	60/62
$p_T^\nu(e)$	$80\,431 \pm 25_{\text{stat}} \pm 22_{\text{syst}}$	71/62
$m_T(\mu,\nu)$	$80\,379 \pm 16_{\text{stat}} \pm 16_{\text{syst}}$	58/48
$p_T^\ell(\mu)$	$80\,348 \pm 18_{\text{stat}} \pm 18_{\text{syst}}$	54/62
$p_T^\nu(\mu)$	$80\,406 \pm 22_{\text{stat}} \pm 20_{\text{syst}}$	79/62

TABLE II. – *Uncertainties for the final combined result on M_W.*

Source	Uncertainty (MeV)
Lepton energy scale and resolution	7
Recoil energy scale and resolution	6
Lepton removal	2
Backgrounds	3
$p_T(W)$ model	5
Parton distributions	10
QED radiation	4
W boson statistics	12
Total	19

Combining all six fits, we obtain a result of

$$M_W = 80\,387 \pm 12_{\text{stat}} \pm 15_{\text{syst}}\,\text{MeV}, \tag{3}$$

or $M_W = 80\,387 \pm 19\,\text{MeV}$. The systematic uncertainties for the combined result are shown in table II. In combination with previous measurements from LEP and the Tevatron, the updated world-average W boson mass is $M_W = 80\,390 \pm 16\,\text{MeV}$. This updated world average impacts the global electroweak fits resulting in a revised upper bound on the Higgs boson mass of $M_H < 145\,\text{GeV}$ at 95% CL.

* * *

The author would like to thank the organizers of La Thuile 2012 for the invitation to speak at a scientifically rewarding and well-organized conference. The author would also like to thank the dedicated team at the CDF Collaboration for the result presented, as well as the many funding agencies worldwide that make the Tevatron research program possible.

REFERENCES

[1] Aaltonen T. *et al.*, *Phys. Rev. Lett.*, **99** (2007) 151801.
[2] Abazov V. *et al.*, *Phys. Rev. Lett.*, **103** (2009) 141801.
[3] Balazs C. and Yuan C.-P., *Phys. Rev. D*, **56** (1997) 5558.
[4] Golonka P. and Was Z., *Eur. J. Phys. C*, **45** (2006) 97.
[5] Carloni Calame C. M. *et al.*, *JHEP*, **10** (2007) 109.
[6] Martin A. D., Stirling W. J., Thorne R. S. and Watt G., *Eur. Phys. J. C*, **63** (2009) 189.
[7] Pumplin J., Stump D., Huston J., Lai H.-L., Nadolsky P. and Tung W.-K., *JHEP*, **07** (2002) 012.
[8] The ALEPH, DELPHI, L3, OPAL, SLD Collaborations, *Phys. Rep.*, **427** (2006) 257.
[9] Lyons L., Gibaut D. and Clifford P., *Nucl. Instrum. Methods A*, **270** (1988) 110.